Supplement of Atmos. Chem. Phys., 24, 911–928, 2024
https://doi.org/10.5194/acp-24-911-2024-supplement

Atmospheric Chemistry and Physics
Open Access
EGU

Supplement of

Low-temperature ice nucleation of sea spray and secondary marine aerosols under cirrus cloud conditions

Ryan J. Patnaude et al.

Correspondence to: Ryan J. Patnaude (ryan.patnaude@colostate.edu)

S1. Estimate of condensation sinks in OFR

In this section, we estimate the ability of vapors to condense onto aerosol particles in order to determine the dominant condensation sinks during the MART experiments. The pSSA and the newly formed SMA particles will compete for the available condensable vapors produced in the MART. The formula to compute the condensation sink CS (s^{-1}), assuming a constant flux correction factor β, is shown in equation (1):

$$CS = \frac{\partial M}{\partial t} = 2\pi\, D_v\, \beta \int D_p\, n\left(D_p\right)\, dD_p \quad (1)$$

where D_v (cm s^{-1}) is the diffusivity coefficient of the condensing vapor. The integral can be simplified into:

$$N\overline{D_p} \quad (2)$$

where N is the total aerosol concentrations and $\overline{D_p}$ is the number mean diameter of the aerosol population. For SMA, N = 10^5 cm^{-3} and for pSSA, N= 150 cm^{-3}. $\overline{D_p}$ was calculated using the geometric mean diameter Dp_g using:

$$\overline{D_p} = Dp_g * \exp\left(0.5 \ln \sigma_g\right)^2) \quad (3)$$

where Dp_g is assumed to be 160 nm and 20 nm, and σ_g is 3.2 and 1.6 for the pSSA and SMA particles, respectively. These lognormal parameters were determined by approximate fitting of lognormal distributions to the aerosol size distributions in Figure S2 (see Figure S6). We assume a D_v of 0.1 cm^2 s^{-1} and the formula for β comes from Dahneke (1983) as reported in Seinfeld & Pandis, (2006), and given by:

$$\beta = \frac{1+Kn}{1+2\,Kn\,(1+Kn)/\alpha} \quad (4)$$

where the accommodation coefficient α is set to 1, and the Knudsen number (Kn) is computed as $2\lambda/\overline{D_p}$ with an assumed λ = 120 nm (Ezhova et al., 2018). Finally, the timescale of condensation for each particle type is determined by taking the inverse of equation 1. This results in estimated condensation sink timescales of ~3 and 11 minutes for the SMA and pSSA, respectively.

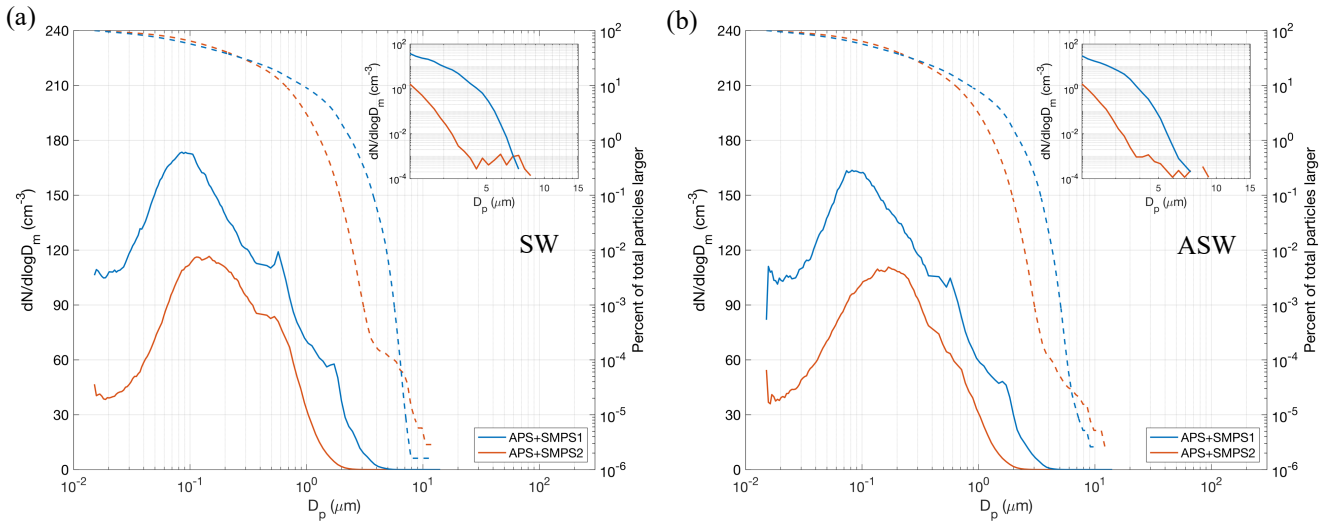

Figure S1 Merged size distributions from the SMPS and APS for the upstream (blue solid line) and downstream (red solid line) set of sizing instruments generated from (a) real and (b) artificial seawater. The dashed lines represent the percent of total particles larger than a given particle diameter and the colors match the size distribution they are referring to. The panels in the upper right of both figures denote the size distributions zoomed in a logarithmic scale for particles > 2 µm.

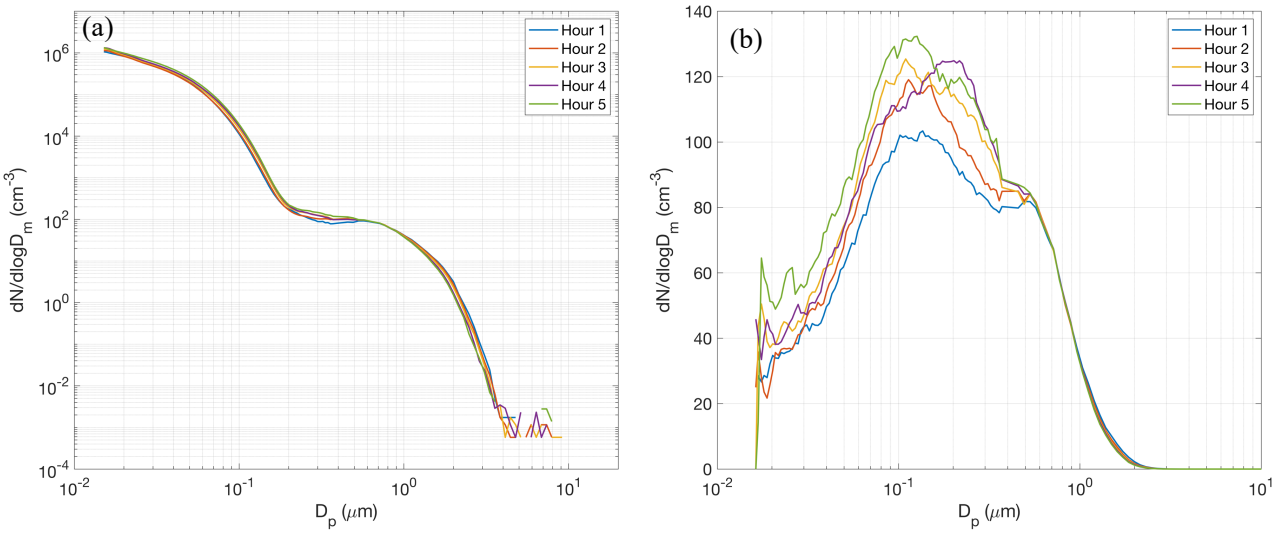

Figure S2. Size distributions of (a) aSSA+SMA and (b) pSSA color-coded by hours of each experiment.

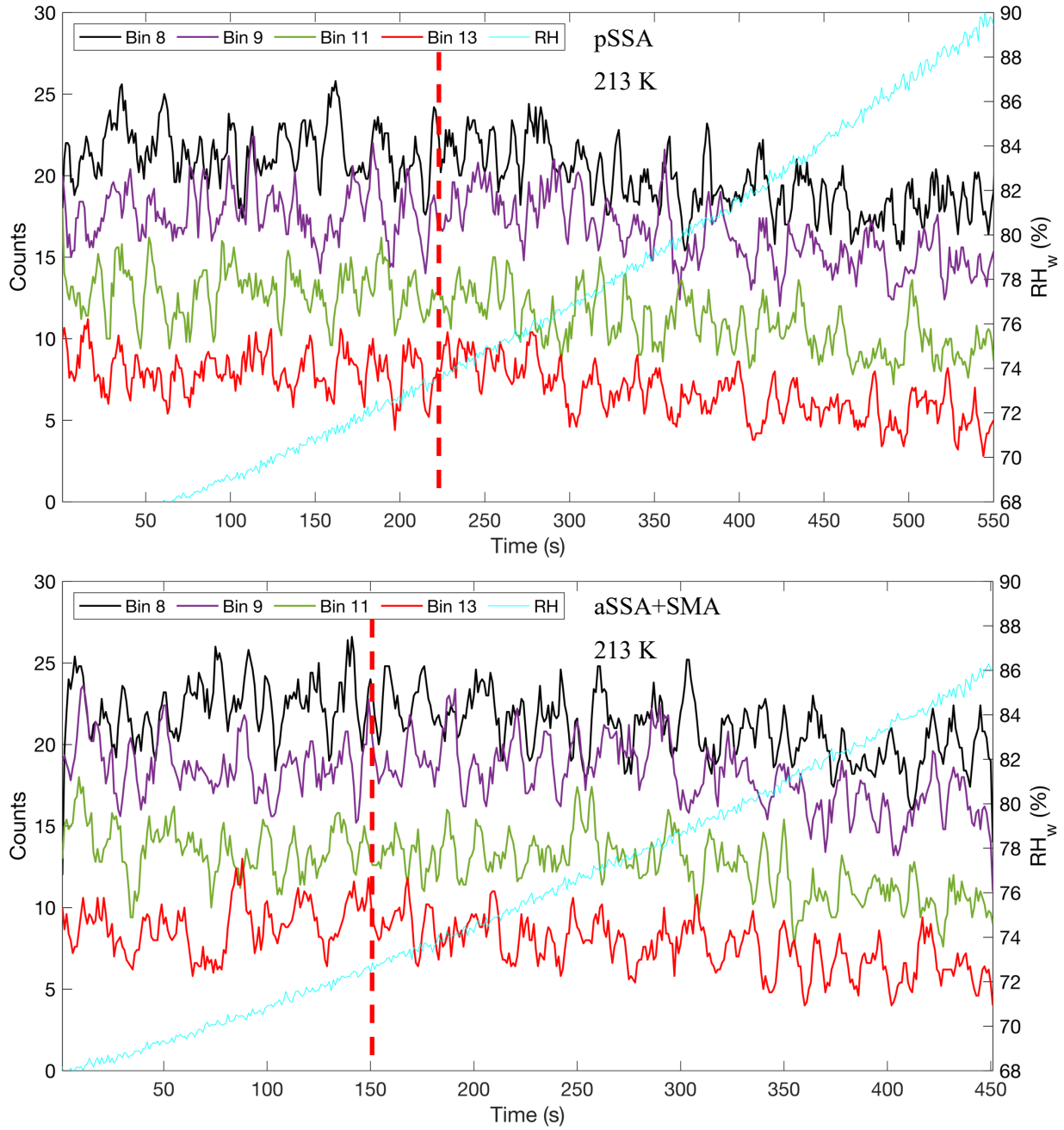

Figure S3. Time series of particle counts for four different OPC size channels for (a) pSSA and (b) aSSA+SMA at 213 K. The cyan line represents the RH_w and the dashed red line represents the RH_w where the particle counts begin to decrease, indicating transfer to larger channels and hence growth by water uptake and particle growth.

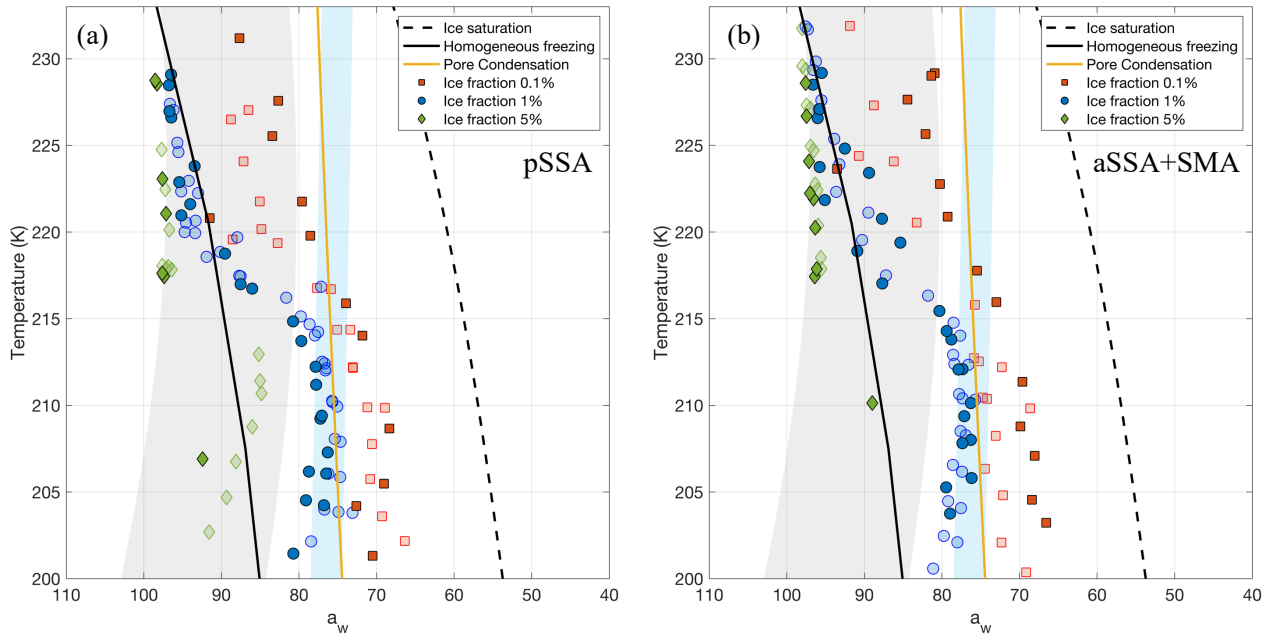

Figure S4. Fraction of frozen particles for (a) pSSA and (b) aSSA+SMA particles. The filled markers denote particles generated from real seawater and the open markers from artificial seawater. The red, blue and green markers indicate 0.1%, 1%, and 5% frozen fractions, respectively. The reference lines indicate ice saturation (black dashed), the parameterized RH_w for pore condensation in an 11 nm pore (Marcolli, 2014) (solid yellow), and the expected threshold for the onset of homogeneous freezing (Koop et al., 2000a) (solid black). The blue shaded region represents the range of possible deliquescence RHs for NaCl and SSA, using the parameterization from Tang & Munkelwitz, (1993) for NaCl extrapolated to colder temperatures as the upper bound and shifting it down 4% RH for SSA following Wagner et al., (2018). The gray shaded region represents the range of uncertainty for the aqueous sulfuric acid particle homogeneous freezing parameterization as presented in Schneider et al. (2021b).

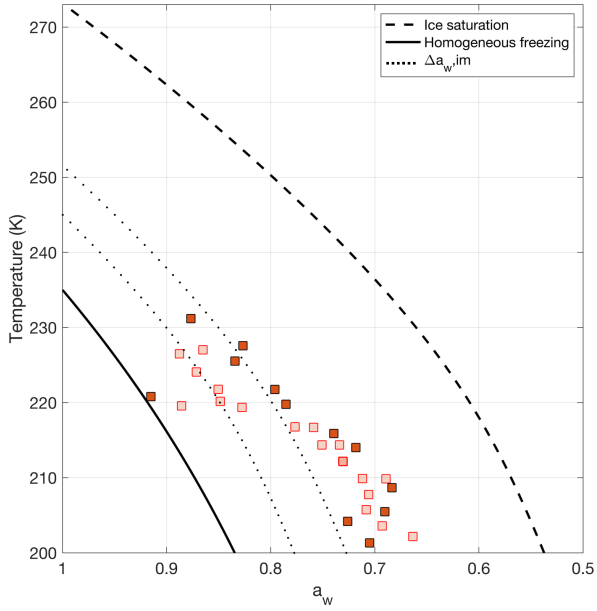

Figure S5 The same 0.1 % frozen fraction shown from Figure S4a, but for a given temperature and water activity (a_w). We assume the larger particles would nucleate ice first leading to a negligible difference between the RH_w and a_w. The reference lines indicate ice saturation (black dashed), the expected threshold for the onset of homogeneous freezing (Koop et al., 2000a) (solid black), and the dotted lines indicates a constant water activity offset (Δa_w) fitted to the 0.1 % data to resemble immersion freezing.

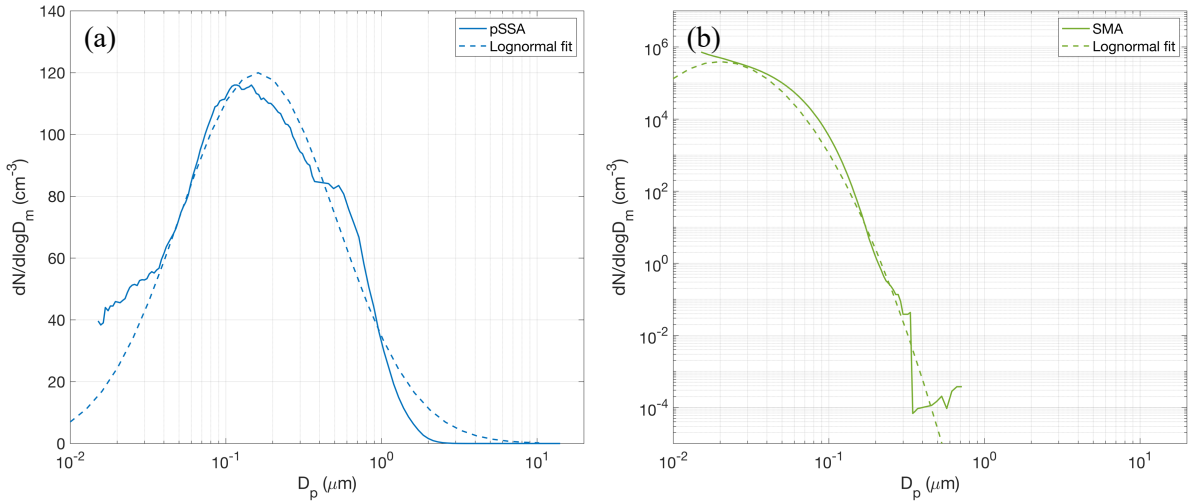

Figure S6. Particle size distributions of (a) pSSA and (b) SMA denoted by the solid lines, which are the same as Figure 2. The dashed lines represent the lognormal fits with geometric mean diameters and σ_g for (a) 160 nm and 3.2 and (b) 20 nm and 1.6, respectively.

References:

Ezhova, E., Kerminen, V.-M., Lehtinen, K. E. J., & Kulmala, M. (2018). A simple model for the time evolution of the condensation sink in the atmosphere for intermediate Knudsen numbers. *Atmospheric Chemistry and Physics*, *18*(4), 2431–2442. https://doi.org/10.5194/acp-18-2431-2018

Dahneke, B. (1983) Simple kinetic theory of Brownian diffusion in vapors and aerosols, in Theory of Dispersed Multiphase Flow, R. E. Meyer, ed., Academic Press, New York, pp. 97-133.

Koop, T., Luo, B., Tsias, A., & Peter, T. (2000a). Water activity as the determinant for homogeneous ice nucleation in aqueous solutions. *Nature*, *406*(6796), 611–614. https://doi.org/10.1038/35020537

Marcolli, C. (2014). Deposition nucleation viewed as homogeneous or immersion freezing in pores and cavities. *Atmospheric Chemistry and Physics*, *14*(4), 2071–2104. https://doi.org/10.5194/acp-14-2071-2014

McCluskey, C. S., Hill, T. C. J., Malfatti, F., Sultana, C. M., Lee, C., Santander, M. V., et al. (2017). A Dynamic Link between Ice Nucleating Particles Released in Nascent Sea Spray Aerosol and Oceanic Biological Activity during Two Mesocosm Experiments. *Journal of the Atmospheric Sciences*, *74*(1), 151–166. https://doi.org/10.1175/JAS-D-16-0087.1

Schneider, J., Höhler, K., Wagner, R., Saathoff, H., Schnaiter, M., Schorr, T., et al. (2021). High homogeneous freezing onsets of sulfuric acid aerosol at cirrus temperatures. *Atmospheric Chemistry and Physics*, *21*(18), 14403–14425. https://doi.org/10.5194/acp-21-14403-2021

Seinfeld, J. H., & Pandis, S. N. (2006). *Atmospheric Chemistry and Phyisics: From Air Pollution to Climate Change. 2nd Edition*., *John Wiley & Sons, Inc.* (Second).

Tang, I. N., & Munkelwitz, H. R. (1993). Composition and temperature dependence of the deliquescence properties of hygroscopic aerosols. *Atmospheric Environment Part A, General Topics*, *27*(4), 467–473. https://doi.org/10.1016/0960-1686(93)90204-C

Wagner, R., Kaufmann, J., Möhler, O., Saathoff, H., Schnaiter, M., Ullrich, R., & Leisner, T. (2018). Heterogeneous Ice Nucleation Ability of NaCl and Sea Salt Aerosol Particles at Cirrus Temperatures. *Journal of Geophysical Research: Atmospheres*, *123*(5), 2841–2860. https://doi.org/10.1002/2017JD027864